A Wireless Network of 8.8-mm³ Bio-Implants Featuring Adaptive Magnetoelectric Power and Multi-Access Bidirectional Telemetry

Zhanghao Yu¹, Wei Wang, Joshua C. Chen, Zhiyu Chen, Yan He, Amanda Singer, Jacob T. Robinson, Kaiyuan Yang²,
Rice University, USA

1zy29@rice.edu, 2kyang@rice.edu

Abstract — This paper presents a hardware platform for wireless mm-sized bio-implant networks, exploiting adaptive magnetoelectric power transfer and novel schemes for efficient bidirectional multi-access communication. The closed-loop power control mitigates power delivery fluctuations caused by distance and alignment change and avoids redundant power of the external transceiver. The system also enables simultaneous power and time-domain modulated downlink data with a 5% peak power transfer efficiency and a 62.3-kbps maximum data rate at 340-kHz carrier frequency; multi-access uplink of all the implants enabled by individually programmed IF with a 40-kbps maximum data rate at 31-MHz carrier frequency; and more than 6-cm distance between the implant and the external TRX.

Keywords — biomedical electronics, implant network, wireless power transmission, wireless biomedical telemetry, magnetoelectric.

I. Introduction

A wireless network of miniaturized battery-less bio-implants with precisely timed sensing and stimulation promises effective and flexible closed-loop and patient-specific control of physiology. By distributing multiple miniaturized implants around the targeted tissue, the envisioned implant network will significantly enhance the flexibility of device deployment, better specificity and spatial resolution, and achieve less infection risks and surgery complexities [1], [2], [3], [4], than current battery-powered single-site implants. Potential clinical applications include multisite spinal cord stimulation, nerve injury rehabilitation and cardiac pacing.

Despite decades of research, wireless power transfer (WPT) and telemetry to bio-implants remains to face critical challenges, which are even more severe for the distributed mm-sized implants. First, the WPT must be robust to ensure the proper operation of all the implants located at different positions and angles, and performing different workloads. Simply generating a strong carrier field may suffer from higher body absorption and shortened battery lifetime of the wearable power TXs [1], [2], [3], [4], [5], [6]. Non-resonant inductive coupling enables regulated WPT [7], but it requires a k_{coupling} greater than $1/Q_{\text{RX}}$, limiting its application in the long-distance WPT for mm-sized implants. Closed-loop control with the help of back telemetry can regulate the received voltage effectively [8], [9]. However, existing demonstrations are all for a single cm-scale RX. Second, simultaneous power and data transfers are desired for higher power efficiency and smaller RX, but is typically



Fig. 1. (a) Conceptual view of the proposed BioNet with adaptive power transfer and bi-directional telemetry and (b) a photo of the 8.8mm³ implants.

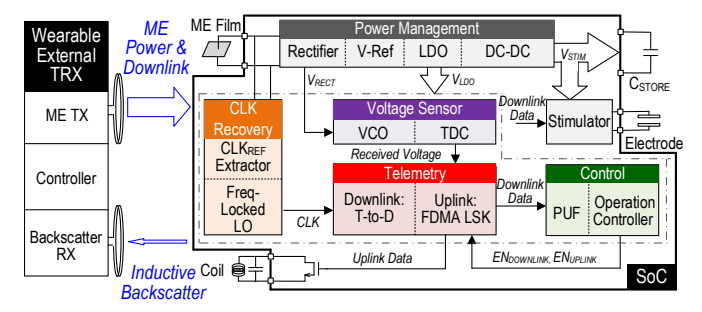


Fig. 2. Block diagram of the bio-implant and the wearable external TRX. restricted by tradeoffs between antenna/transducer quality factor and bandwidth [3], [10], [11], [12], [13]. Third, efficient and robust multi-access telemetries in both directions are indispensable in distributed implant networks.

To tackle these challenges, we present BioNet, a wireless network of mm-sized implants with closed-loop adaptive magnetoelectric power transfer regulation and novel schemes for efficient and robust multi-access bidirectional communication (Fig. 1 (a)). The BioNet of the 8.8-mm³ implants (Fig. 1 (b)) features: (1) closed-loop magnetoelectric wireless power transfer that adapt to implants' workload, and changes of their distances and misalignments to the external TRX; (2) simultaneous power and time-domain downlink telemetry with a 5% peak power transfer efficiency (PTE) and a 62.3-kbps maximum data rate; (3) multi-access uplink telemetry enabled by individually programmed intermediate frequency (IF); (4) robust operation under 2-V source variations; and (5) a > 6-cm TRX-implant working distance to receive > 1.3-V power input and support 62.3-kbps downlink and 40-kbps uplink data rates.

II. SYSTEM OVERVIEW

The proposed BioNet system includes an external TRX consisting of a magnetoelectric (ME) power TX, a backscatter

RX and a microcontroller to power and communicate all the implants and perform global WPT regulation (Fig. 2). Each implant integrates a 1-mm² SoC, a 4x2-mm² ME transducer, a 2.5-mm² backscattering coil with conjugate impedance matching, and an 0.25-mm³, 22-µF capacitor storing a maximum energy of 135-µJ. The implant SoC recovers multiple supply voltages from ME and performs bidirectional telemetry, clock recovery, input voltage sensing, and stimulation with control of the external TRX.

Magnetoelectric WPT that converts sub-MHz magnetic field to AC voltage by a mm-sized thin-film transducer is promising for miniature implants. It offers superior misalignment tolerance, lower tissue absorption and safe mW-level power delivery with higher PTE than inductive coupling and ultrasonic approaches [4], [10]. A recent study also shows that a single ME TX could power multiple implants [4]. To leverage the advantages of ME WPT while enabling simultaneous power and data transfer, the BioNet adopts a hybrid scheme with ME power and downlink (DL) and inductive backscattering uplink (UL). Both modalities are based on AC magnetic fields, simplifying the system integration.

III. SYSTEM IMPLEMENTATIONS

A. Downlink Data with Time-Domain Modulation

Simultaneous power transfer and telemetry are highly desirable for implants with little energy storage. OOK [11], ASK-PPM [6], and ASK-PWM [3], [12] require frequent amplitude switching, leading to input power fluctuations and low data rates constrained by the high quality factor of antenna/transducer (Fig. 3 (a)). Frequency splitting FSK is recently proposed for stable power delivery and high data rate [13]. However, it requires strong coupling that is sensitive to distance changes and misalignment (Fig. 3 (b)).

Here, we propose a notch-spacing time-domain modulation scheme, where multiple bits are encoded into the duration of a pulse for amortizing the transducer's low switching speed (Fig. 3 (c)). Each pulse is defined by two narrow magnetic field notches, which can be quickly detected by the active rectifier's comparators [4]. This method minimizes PTE reduction. Considering the tradeoff between switching

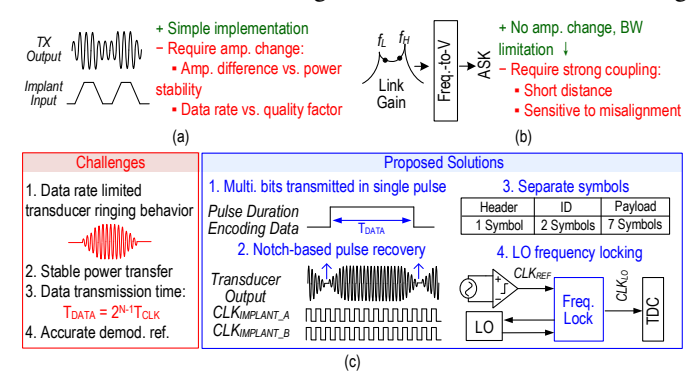


Fig. 3. Existing modulation schemes for simultaneous wireless power and data transfer: (a)OOK, ASK-PWM, and ASK-PPM and (b) frequency splitting FSK; and (c) proposed notch-spacing time-domain modulation.

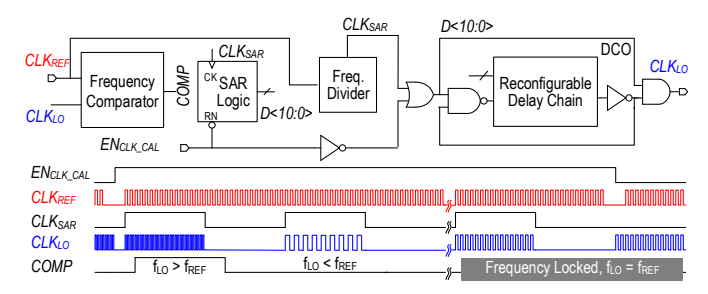


Fig. 4. Schematics and operation waveforms of the frequency-locking-based local timing reference generation

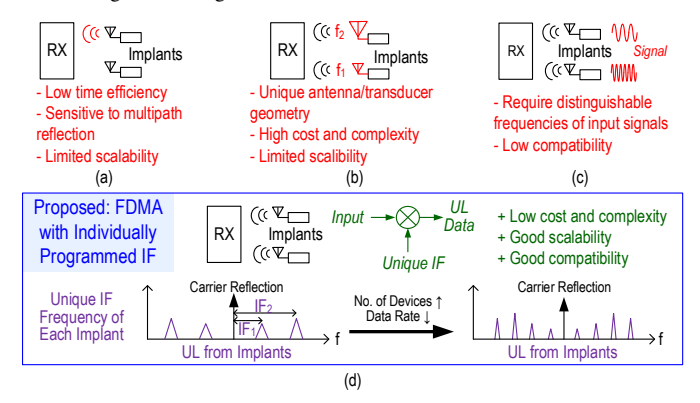


Fig. 5. Existing multiple-access uplink telemetry strategies: (a) TDMA, (b) FDMA with different carrier frequency, and (c) FDMA with analog modulation; and (d) principles of the proposed FDMA with individually programmed IF.

time amortization and duration encoding overheads, each data symbol is designed to contain at most 6 bits. A complete packet includes a header, an ID for individual addressing, and a payload. An accurate clock is critical for correct demodulation. While recovering a PVT-invariant clock from the source is straightforward, it fails when the carrier field is absent and thus incompatible with the notch-based scheme. To address this, an LO in each implant is frequency locked to the clock recovered from the source ($CLK_{\rm REF}$) as the timing reference ($CLK_{\rm LO}$) for demodulation. The frequency locking is autonomously performed before each downlink data transfer session with SAR logic (Fig. 4).

B. Uplink Backscatter with FDMA

In BioNet, accessing every implant's feedback is essential, which requires a multi-access uplink. FDMA is preferred over TDMA [3] for higher timing efficiency. However, the existing FDMA uplink for multiple implants requires different carrier frequencies [1] or input signal frequencies [2], limiting their scalability and compatibility (Fig. 5 (a), (b) and (c)).

Using IF has shown benefits for SNR in inductive backscatter [14]. This work further leverages IF to realize low-cost, scalable FDMA in backscatter by mixing the individually programmed IF with the uplink data (Fig. 5 (d)). With this mechanism, all implants are accessible to the external TRX simultaneously [15]. The data rate of the implants is programmed based on the channel condition to optimize SNR. The uplink module consists of a VCO-based quantizer for implant voltage $V_{\rm RECT}$ sensing (Fig.6 (a)), a TDC, a

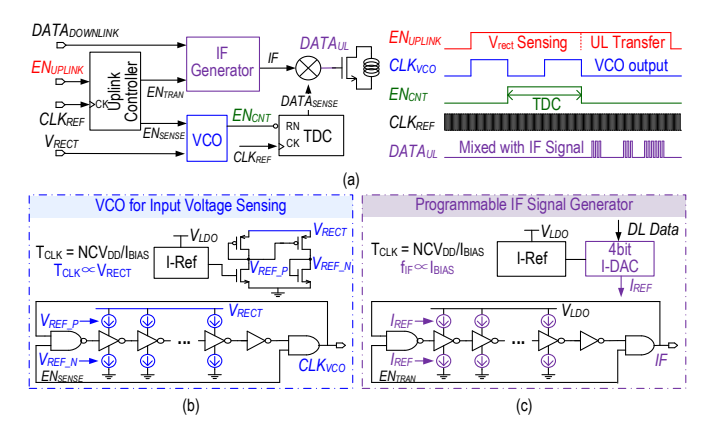


Fig. 6. (a) Schematics of the FDMA backscatter circuity and the operating waveform; (b) schematic of the VCO for implant input voltage sensing; and (c) schematic of the programmable IF signal generator.

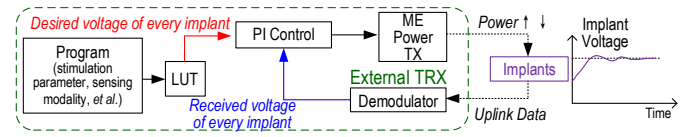


Fig. 7. Block diagram of the proposed closed-loop global power control. controller, and an IF generator, which is a programmable current-starved oscillator with uniform tuning steps (Fig.6 (b)).

C. Adaptive global power transfer control

With the help of on-chip PUF IDs, each implant's functionalities are individually programmed and controlled by the external TRX, which knows the received power of each implant though the multi-access uplink. The TRX adapts the power TX's output power to regulate the implant's input power based on its real-time workload and the channel efficiency. The proposed closed-loop control of WPT can significantly mitigate power delivery fluctuations led by varying distance and misalignment and avoid unnecessary power consumption of the external TRX under light workloads.

IV. MEASUREMENT RESULTS

The implant SoC is fabricated in TSMC 180-nm CMOS technology (Fig. 8 (a)). The BioNet system is measured *in vitro* with a 2-cm-thick porcine tissue (Fig. 8 (b) and (c)).

The implants continuously receive power during the downlink and uplink data transfer (Fig. 9 (a)). Device

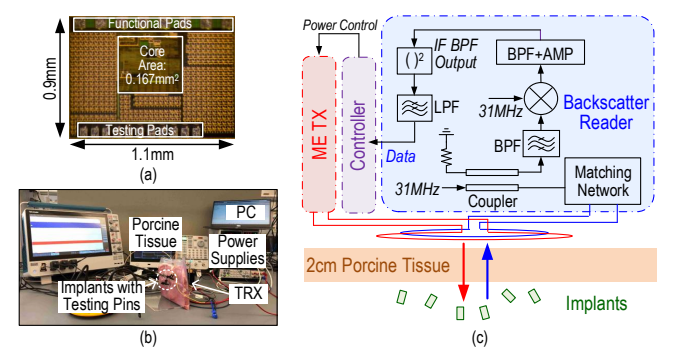


Fig. 8. (a) Implant chip micrograph; (b) illustration of the *in-vitro* test with 2-cm porcine tissue and (c) schematics of the external TRX's backscatter RX and the *in-vitro* test setup.

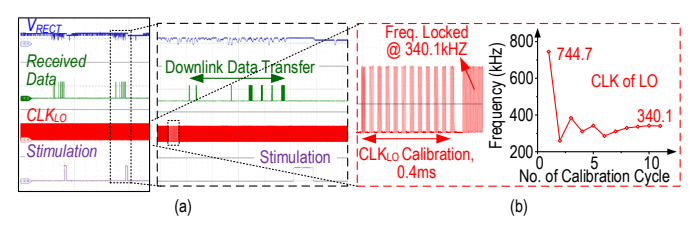


Fig. 9. (a) Measured waveforms of the implant's normal operation with simultaneous power and downlink data transfers; and (b) zoom-in view of the measured frequency calibration of clock recovery.

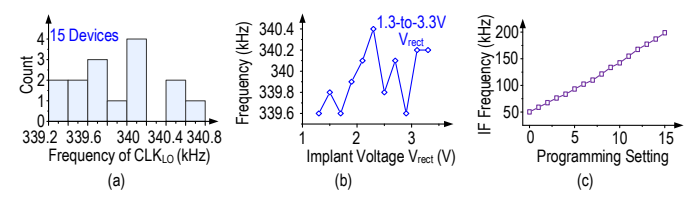


Fig. 10. Measured clock $CLK_{\rm LO}$ locking of (a) 15 devices and (b) with 1.3-to-3.3-V input voltages variations; and (c) measured IF frequency with individual downlink programming.

programming downlink data is decoded by a self-calibrated timing reference $CLK_{\rm LO}$. The LO accurately locks to the 340.1-kHz carrier frequency in 0.4 ms (Fig. 9 (b)). The measured $CLK_{\rm LO}$ shows 0.2% maximum error across a 2-V input voltage change in 15 devices, proving its robustness to process and voltage variations (Fig. 10 (a), (b)). For instance, the IF oscillator for data uplink can be programmed in the 50-to-200-kHz range (Fig. 10 (c)).

Fig. 11 shows the operation waveform of the uplink telemetry and the sensing and reporting of implant's received voltage. The system's uplink achieves a BER of 5.5E-5 through the 2-cm porcine tissue when transmitting a 40-kbps PRBS with a 0-dBm backscatter RX coil power (Fig. 12 (a)). Furthermore, multi-access uplink is illustrated by the spectrum of two implants transmitting data simultaneously at distinct, individually programmed IF of 83 and 108 kHz (Fig. 12 (b)).

Fig. 13 demonstrates the continuous closed-loop WPT regulation with changing TRX-implant distance. With a 1.5-cm distance increase, ME voltage drops from 2.8 V to 1.52 V,

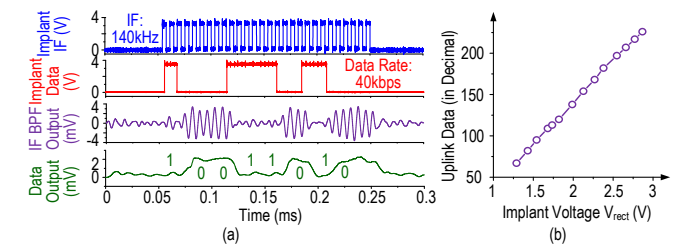


Fig. 11. (a) Measured waveforms of uplink data demodulation with 140-kHz IF frequency and 40-kbps data rate and (b) implant voltage feedback.

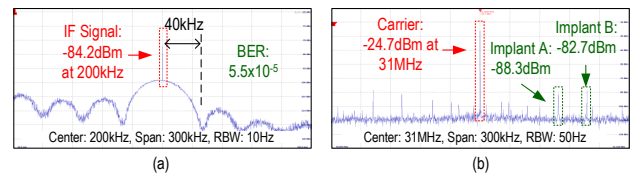


Fig. 12. Spectrums of the uplink tested with (a) 40-kbps PRBS and (b) simultaneous backscattering of two implants whose uplink IF frequencies are individually programmed, all tests are conducted *in vitro*.

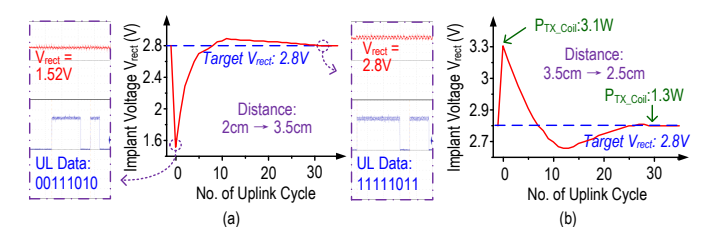


Fig. 13. Measured sample operations of global wireless power transfer control against device movements: external TRX-implant distance (a) increases from 2 cm to 3.5 cm and (b) decreases from 3.5 m to 2.5 cm.

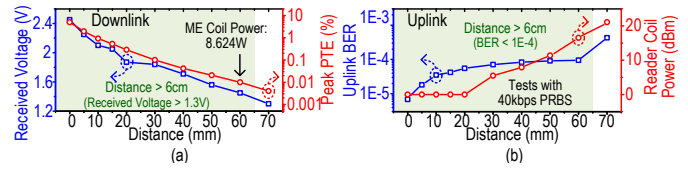


Fig. 14. Measured (a) received voltage, power transfer efficiency and (b) uplink BER at various distances between the external TRX and the implant.

resulting in a maximum 1.38-mW reduction of received power. The implant's voltage then resumes to the desired 2.8 V after 30 tuning cycles with adaptive control of the ME TX's power. When the distance decreases from 3.5 cm to 2.5 cm, the regulation loop saves 1.8 W (i.e. 58%) of ME TX coil power.

The implant is fully functional (i.e., receiving > 1.3 V from ME WPT and achieving < 1E-4 uplink BER) at 6 cm away from the TRX without violating IEEE safety limits (a maximum TX coil power of 17.6 W at 340 kHz in COMSOL) (Fig. 14). In comparison with mm-sized state-of-the-art [3], [5], [11], the proposed work achieves the best PTE and the largest operating distance. Due to the time-domain modulation, its ratio of data rate/ $f_{\rm carrier}$ in downlink is much higher than [3], [11] and comparable with [13], which operates with a much smaller distance. It enables FDMA in uplink with individually programmed IF (Table 1).

Table 1. Comparison with state-of-the-art integrated power and telemetry platforms for wireless bio-implants

		This	Nat.	JSSC'19	CICC'19	VLSI'21	CICC'20	ISSCC'21	ISSCC'21
		Work	BME'20 [5]		[3]	[12]	[11]	[13]	[9]
Technology		180	65	65	65	180	180	180	180
Bio-Function		Stimulation	Stimulation	Recording	Recording	Recording	No	No	No
Power	Link	ME	Ultrasonic	Ultrasonic	Inductive	Optical	Inductive	Inductive	Inductive
	Harvester Size	0.8mm ³ ME Film	0.4mm ³ Piezo	0.6mm ³ Piezo	0.25mm ² Coil	N/A	4mm ² Coil	706mm ² Coil	462mm ² Coil
	Peak PTE at Distance (mm)	5% at 0 0.2% at 20	0.06% at 18	N/A	0.06% at 10	N/A	1.04% at 1	89.6% at 5	N/A
	Global Control?	Yes	No	No	No	No	No	No	Yes
DL Data	Link	ME	Ultrasonic	N/A	Inductive	Optical	Inductive	Inductive	
	f _{carrier} (MHz)	0.34	1.85		900	N/A	27	6.5, 7.5	
	Modulation Scheme	Time Modulation	AM		ASK- PWM	ASK- PWM	ASK	FSK	
	Data Rate (kbps)	Max: 62.3	N/A		1000	N/A	6.6	2500	N/A
	DR/f _{carrier}	0.18	N/A		0.0011	N/A	0.00024	0.38	
	Individually Addressable?	Yes	No		Yes	Yes	No	No	
UL Data	Link	Inductive	Ultrasonic	Ultrasonic	Inductive	Optical	Inductive	N/A	Inductive
	f _{carrier} (MHz)	31	1.85	1.78	900	N/A	700		6.78
	Scheme	LSK	LSK	LSK	LSK	PWM	LSK		LSK
	Data Rate (kbps)	40	N/A	35	10000	0.3	27000		N/A
	Multiple Access?	FDMA with Programmable IF	No	FDMA w Diff. f _{INPUT}	TDMA	No	No		No
	BER	1.00E-04	N/A	N/A	N/A	N/A	1.00E-04		N/A
SoC Power (µW)		11	4	37.7	N/A	0.57	N/A	N/A	N/A
Implant Size (mm ³)		8.8	1.7	0.8	N/A	N/A	N/A	N/A	N/A
Max. Distance (mm)		60	55	50	10	N/A	2.5	5	N/A

V. CONCLUSION

This paper presents a wireless network of mm-sized implants exploiting adaptive biomedical closed-loop control of ME power transfer and novel schemes for multi-access bidirectional communications. The adopted global WPT control significantly improves the robustness against perturbations of distance and alignment and the system's overall efficiency. The time-domain modulated downlink works simultaneously with the power transfer, and achieve a 5% peak power transfer efficiency and a 62.3-kbps maximum data rate. FDMA uplink is realized by individually programmed IF with a maximum data rate of 40 kbps. The system is tested in vitro and has a > 6-cm working distance between the external TRX and the implant.

ACKNOWLEDGMENT

This research was in part sponsored by the National Science Foundation (NSF) under ECCS-2023849 and the Defense Advanced Research Projects Agency (DARPA) under FA8650-21-2-7119. The views, opinions and/or findings expressed are those of the author and should not be interpreted as representing the official views or policies of the Department of Defense or the U.S. Government.

REFERENCES

- A. Khalifa et al., "The Microbead: A Highly Miniaturized Wirelessly Powered Implantable Neural Stimulating System," TBioCAS, Jun. 2018.
- [2] M. M. Ghanbari et al., "A Sub-mm³ Ultrasonic Free-Floating Implant for Multi-Mote Neural Recording," JSSC, Nov. 2019.
- [3] V. W. Leung et al., "Distributed Microscale Brain Implants with Wireless Power Transfer and Mbps Bi-directional Networked Communications," in CICC, Apr. 2019.
- [4] Z. Yu et al., "Multisite bio-stimulating implants magnetoelectrically powered and individually programmed by a single transmitter," in CICC, Apr. 2021.
- [5] D. K. Piech et al., "A wireless millimetre-scale implantable neural stimulator with ultrasonically powered bidirectional communication," Nat. Biomed. Eng., Feb. 2020.
- [6] Y. Jia et al., "A mm-sized free-floating wirelessly powered implantable optical stimulating system-on-a-chip," in ISSCC, Feb. 2018.
- [7] J. Pan *et al.*, "An inductively-coupled wireless power-transfer system that is immune to distance and load variations," in *ISSCC*, Feb. 2017.
- [8] X. Li et al., "A 13.56 MHz Wireless Power Transfer System With Reconfigurable Resonant Regulating Rectifier and Wireless Power Control for Implantable Medical Devices," JSSC, Apr. 2015.
- [9] J. Tang et al., "A Wireless Power Transfer System with Up-to-20% Light- Load Efficiency Enhancement and Instant Dynamic Response by Fully Integrated Wireless Hysteretic Control for Bioimplants," in ISSCC, Feb. 2021.
- [10] Z. Yu et al., "MagNI: A Magnetoelectrically Powered and Controlled Wireless Neurostimulating Implant," TBioCAS, Dec. 2020.
- [11] J. Thimot et al., "A 27-Mbps, 0.08-mm³ CMOS Transceiver with Simultaneous Near-field Power Transmission and Data Telemetry for Implantable Systems," in CICC, Mar. 2020.
- [12] J. Lim et al., "A Light Tolerant Neural Recording IC for Near-Infrared-Powered Free Floating Motes," in VLSI, Jun. 2021.
- [13] Y. Park et al., "A Frequency-Splitting-Based Wireless Power and Data Transfer IC for Neural Prostheses with Simultaneous 115mW Power and 2.5Mb/s Forward Data Delivery," in ISSCC, Feb. 2021.
- [14] N.-C. Kuo et al., "Inductive Wireless Power Transfer and Uplink Design for a CMOS Tag With 0.01 mm² Coil Size," Microw. Wirel. Compon. Lett., Oct. 2016.
- [15] D. Yeager, W. Biederman, N. Narevsky, E. Alon, and J. Rabaey, "A fully-integrated 10.5μW miniaturized (0.125mm²) wireless neural sensor," in Symposium on VLSI Circuits, Jun. 2012.